Performance Evaluation of Poly(amide-imide) Incorporated Cellulose Acetate Ultrafiltration Membranes in the Separation of Proteins and Its Fouling Propensity by AFM Imaging

ARTICLE *in* INDUSTRIAL & ENGINEERING CHEMISTRY RESEARCH · NOVEMBER 2011

Impact Factor: 2.59 · DOI: 10.1021/ie201181h

I&EC research
Industrial & Engineering Chemistry Research

ARTICLE

pubs.acs.org/IECR

Performance Evaluation of Poly(amide-imide) Incorporated Cellulose Acetate Ultrafiltration Membranes in the Separation of Proteins and Its Fouling Propensity by AFM Imaging

Sahadevan Rajesh,[†] Ayyavoo Jayalakshmi,[†] Sundararaj Senthilkumar,[†] H. S. Hari Sankar,[‡] and Doraiswamy R. Mohan*[,†]

[†]Membrane Laboratory, Department of Chemical Engineering, Anna University Chennai, Chennai-600 025, India

[‡]Inter University Center for Development of Marine Bio-Technology, School of Marine Sciences, CUSAT, Cochin-682 016, India

ABSTRACT: Polymeric membranes intended to be used in protein separation must be fouling resistant in order to reduce the interactions with proteins during operation. Therefore, cellulose acetate (CA) membranes with superior properties were prepared by phase inversion technique using high-performance thermoplastic poly(amide-imide) (PAI) as the modification agent. The prepared membranes were characterized using attenuated total reflectance Fourier transform infrared spectroscopy (ATR-FTIR), scanning electron microscopy (SEM), atomic force microscopy (AFM), molecular weight cutoff, and pore size to investigate the influence of PAI on the properties of the resultant membranes. Intermolecular interactions between the components in blend membranes were established by ATR-FTIR and SEM analysis showed that the blend CA membranes have thinner top layer and higher porosity in the sublayer. These prepared membranes were subjected to the separation of proteins such as bovine serum albumin, egg albumin, pepsin, and trypsin. The fouling-resistant capability of the membranes was studied by bovine serum albumin as the model protein and increase in resistance during protein filtration was calculated by means of resistance in series model analysis. The fouled membranes were characterized by AFM imaging and these membranes were cleaned by washing with deionized water and subsequent sonication. From the AFM images of the fouled membranes it was clear that preferential adsorption takes place at specific locations on the membrane surface and is a function of surface roughness and membrane hydrophilicity. It is worth mentioning that the incorporation of poly(amide-imide) into the cellulose acetate matrix is an effective method for the development of low fouling ultrafiltration membranes for the separation of proteins.

1. INTRODUCTION

Membrane technology has become an attractive alternative to many energy-intensive separation processes because separation using membranes does not require additives and can be performed isothermally at low temperatures with minimum energy consumption.[1−3] Although all membrane processes are used for bioseparation, ultrafiltration (UF) has gained importance in biotechnology due to its ability of size- and charge-based separation with high purity and throughput.[4,5] Intensive research has been carried out by several researchers on the transmission and rejection of proteins using cellulose acetate and polysulfone membranes and confirmed the reliability of the process of ultrafiltration in macromolecular separations. But the application of UF in the separation of proteins is limited due to the tendency of the proteins to foul the membranes by adsorption and deposition.[6−8] Current research and development efforts are directed toward drastic improvements in the antifouling property while maintaining the inherent high-throughput characteristics of the membranes.[9]

In membrane separation, fouling is defined as a flux decline and reduced transmission over time resulting from the reversible accumulation of solutes at the membrane surface progressing to irreversible adsorption and cake buildup.[10,11] The main factors that influence fouling are the hydrodynamics of the process and the physicochemical properties of the membranes and feed solutions. Generally, proteins are adsorbed more strongly at hydrophobic surfaces than hydrophilic surfaces because of hydrophobic interaction.[12,13] A fundamental understanding of such interactions at clean and fouled membrane surface is important in the understanding and optimization of the protein separation in biotechnology.[14−16] Therefore, the present investigation is focused on the improvement of membrane fouling resistance by increasing the hydrophilicity of the neutral membrane for protein separation applications.

Since the development of asymmetric membranes, cellulose acetate (CA) has been considered as an important membrane material because of advantages such as moderate flux, high salt rejection properties, and renewable source of raw material.[17−19] The requirement for more chemical- and mechanical-resistant membranes and aggressive cleaning led to the necessity of modified CA based membranes. The hydrophilic/hydrophobic balance as well as the physico−chemical properties of the CA membranes can be improved by means of blending with a suitable polymer. CA has been blended with several high-performance polymers such as poly(sulfone), poly(ethersulfone), poly(ether ether ketone), and poly(etherimide) for improving the CA membrane properties and was found to be successful.[6,17,20−22]

Recently, aromatic poly imides have attracted interest as promising membrane materials because of their excellent chemical, mechanical, and thermal stabilities.[7,23,24] However, there are

Received: June 2, 2011
Accepted: November 8, 2011
Revised: September 21, 2011
Published: November 08, 2011

dx.doi.org/10.1021/ie201181h | *Ind. Eng. Chem. Res.* 2011, 50, 14016–14029

some limitations on selecting suitable solvents in preparing asymmetric membranes via the traditional phase inversion process, since polyimide materials are normally resistant to solvent dissolution. The processability and solubility of the polyimide can be improved by the inclusion of amide group in the imide backbone. Thus aromatic poly(amide-imide) (PAI) appears to be of particular interest as a membrane material in view of the fact that the aromatic imide units provide the high-performance properties while flexible ether linkages provide good processability.

The present study is one of our series of investigations into the preparation of poly(amide-imide) incorporated CA ultrafiltration membranes and its characterization. This study focuses on the effects of CA/PAI blend composition and water-soluble additive PEG-600 on the rejection and permeate flux of proteins such as bovine serum albumin (BSA), egg albumin (EA), pepsin, and trypsin. The fouling-resistant capability of the membranes was studied by bovine serum albumin as the model protein and increase in resistance during protein filtration was calculated by means of resistance in series model analysis. The fouled membranes were characterized by AFM imaging and these membranes were cleaned by means of washing with deionized water and subsequent sonication. Attempts have been made to correlate the changes in protein separation efficiency and fouling resistance properties of the CA/PAI membranes with morphology. Flux recovery ratio (FRR) values of the pure CA and CA/PAI blend membranes were calculated and the results are discussed.

2. EXPERIMENTAL SECTION

2.1. Materials and Methods. Commercial-grade MYCEL cellulose acetate CDA5770 (glass transition temperature 219 °C and acetyl content 39.99%) was procured from Mysore Acetate and Chemicals Company Limited., India, and was used after recrystallization from acetone. Commercial-grade poly(amide-imide), Torlon 4000T-HV, (glass transition temperature 285 °C) supplied as gift sample by Solvay Advanced Polymers, LLC, USA, was used as received.

Analar grade *N*-methyl-2-pyrrolidone (NMP) from SRL Chemicals Ltd., India, was sieved through molecular sieves (Type 5A°) to remove moisture and stored in dry condition prior to use. Sodium lauryl sulfate (SLS) of analar grade was obtained from Qualigens Fine Chemicals Ltd., India, and was used as surfactant in the coagulation bath. Polyethylene glycol 600 (PEG 600) was procured from Merck (I) Ltd., and was used as supplied as a nonsolvent additive for the whole study. Anhydrous sodium monobasic phosphate and sodium dibasic phosphate hepta hydrate were procured from SRL Chemicals Ltd., India, and used for the preparation of phosphate buffer solution for the protein analysis. Distilled water was employed for the ultrafiltration experiments and for the preparation of gelation bath. Proteins, viz., bovine serum albumin (BSA), M_w = 69 KDa; pepsin M_w = 35 KDa; and trypsin, M_w = 20 KDa, were purchased from SRL Chemicals Ltd., Mumbai, India, and used as received. Egg albumin (EA), M_w = 45 KDa, was obtained from CDH Chemicals Mumbai, India.

2.2. Preparation of Blend Membranes. The blend solutions based on CA and PAI (total polymer concentration = 17.5 wt %) was prepared by dissolving the two polymers in different compositions in the absence and presence of additive PEG600 in NMP under constant mechanical stirring in a round-bottomed flask for 4 h at 40 °C. A series of such polymer solutions was prepared by varying the composition of CA and PAI with PEG-600, as shown in Table 1. The homogeneous solution thus obtained was allowed to stand at room temperature for at least 6 h in an airtight condition to get rid of air bubbles. The preparation method involved is the same as that of the "phase inversion" method employed in our earlier works as reported by other researchers.[25,26]

Table 1. Composition and Casting Conditions of CA/PAI Blend Membranes[a]

blend composition			
cellulose acetate (wt%)	poly(amide-imide) (wt%)	additive, PEG 600 (wt %)	solvent, NMP (wt %)
100	0	0	82.5
90	10	0	82.5
80	20	0	82.5
70	30	0	82.5
100	0	2.5	80.0
90	10	2.5	80.0
80	20	2.5	80.0
70	30	2.5	80.0

[a] Casting temperature 30 ± 1° C; casting relative humidity 25 ± 2%; solvent evaporation time 30 sec. Total polymer concentration at 17.5 wt %.

2.3. Experimental Setup. The ultrafiltration permeation experiments were carried out in a batch-type, dead-end cell (UF cell 8400, Amicon, USA) with an internal diameter of 76 mm fitted with a Teflon-coated magnetic paddle. The cell was connected to a compressor with a pressure control valve and gauge through a feed reservoir. The schematic representation of the ultrafiltration experimental setup has been given elsewhere.[25] The effective membrane area available for ultrafiltration was 38.5 cm^2. All the experiments were carried out at 30 ± 2 °C and a transmembrane pressure of 345 kPa.

2.4. Membrane Characterization. *2.4.1. FTIR Analysis.* FTIR spectra of pure CA and CA/PAI blend membranes were recorded using an attenuated total reflectance (ATR) technique with a spectrometer (Thermo Nicolet, Avatar 370) in the range of 500−4000 cm^{-1}. The IR spectrum for the pure PAI powder was obtained by the KBr pellet method.

2.4.2. Scanning Electron Microscopy (SEM) Analysis. The cross-sectional images of the CA and CA/PAI blend membranes were taken by scanning electron microscope (SEM, Cam Scan MV2300). The membranes were cut into small pieces and cleaned with blotting paper. The pieces were immersed in liquid nitrogen for 60−90 s and were frozen. These frozen fragments of the membranes were stored in a desiccator. The dried samples were gold sputtered for producing electric conductivity and photographs were taken in very high vacuum conditions.

2.4.3. Atomic Force Microscopy (AFM) Analysis. Atomic force microscopy was used to analyze the surface morphology and roughness of the prepared membranes (AFM device was a Dual Scope scanning probe-optical microscope, DME model C-21, Denmark). Small squares of the prepared membranes (approximately 1 cm^2) were cut and glued on a glass substrate. The membrane surfaces were imaged in a scan size of 1 μm × 1 μm and the surface roughness were measured by tapping mode, since the contact mode AFM cannot be applied to polymeric membranes because of the excessive tracking forces applied to the sample by the probe.

2.4.4. Protein Rejection Studies. Protein solutions of BSA, EA, pepsin, and trypsin were prepared (0.1 wt %) in phosphate buffer (0.5 M, pH 6.0) and used as a standard solution for the rejection studies. Filtration through each membrane was carried out individually and concentration of the feed solution was kept constant throughout the run. The permeate protein concentration, collected over different time intervals, was estimated using a UV−visible spectrophotometer (Hitachi, model U-2000) at a wavelength of 280 nm. The percentage of protein rejection was calculated from the concentration of the feed and the permeate using eq 1

$$\%\text{proteinrejection} = \left[1 - \left(\frac{C_p}{C_f}\right)\right] \times 100 \quad (1)$$

where C_f and C_p are the concentration of protein in the feed and permeate solution, respectively.

The protein solution permeate flux is determined as follows:[27]

$$J_w = \frac{Q}{A(\Delta t)} \quad (2)$$

where J_w is the protein flux (in $lm^{-2}\ h^{-1}$), Q is the quantity of protein permeate in liters; Δt is the sampling time (in h), and A is the membrane area (in m^2).

2.4.5. Molecular Weight Cutoff and Pore Size. Molecular weight cutoff (MWCO) and pore size of the prepared membranes were calculated by performing sieving experiments with dilute protein solutions of different molecular weight.[28] The MWCO has a linear relationship with the pore size of the membrane. In general, the MWCO of the membrane is determined by identifying an inert molecule of lowest molecular weight that has a solute rejection of more than 80% in steady state UF experiments.[21] MWCO of individual membranes was calculated by the values obtained from the protein rejection experiments conducted earlier. The radius of the protein molecule used for the rejection was determined from their diffusion coefficient using Stokes−Einstein equation and this enables us to calculate the average pore radius of the membranes[3]

$$r_{(nm)} = 0.88(\text{MW})^{1/3} \quad (3)$$

where $r_{(nm)}$ is the radius of the membrane pore in nanometer and MW is the molecular weight of the protein in Kilo Dalton.

2.4.6. Fouling Analysis. BSA solution (0.1 wt %) was prepared with 0.5 M phosphate buffer solution (pH 6.0) and used as feed solution for the fouling studies. Each membrane was initially compacted for 30 min and the pure water flux, J_{w1}, was measured at a transmembrane pressure of 345 kPa, according to eq 2. The cell was then emptied and refilled with BSA solution and protein solution flux, J_p, after 4 h of filtration was recorded. To evaluate the antifouling property of CA/PAI blend membranes, the flux decline rate was calculated by the following equation:[9,29]

$$R_{fd} = \left[1 - \frac{J_p}{J_{w1}}\right] \times 100 \quad (4)$$

A high value of R_{fd} corresponds to a large flux decay and severe membrane fouling.

2.4.7. Fouling Evaluation by Resistance in Series Model. For a pressure-driven filtration process the permeation of pure water across a membrane can be described by Darcy's law.[2,30]

$$\frac{d(v)}{dt} = J_w = \frac{\Delta p}{\mu R_m} \quad (5)$$

Where J_w ($m^3\ m^{-2}\ s^{-1}$) is the permeate flux, ΔP is the transmembrane pressure (Pa), μ is the viscosity of water (Pa s), and R_m is the intrinsic membrane resistance (m^{-1}). However, in suspension filtration, the permeate flux will always be less than that given in the above equation. Flux decline is a result of the increase of membrane resistance to the permeate flow, resulting from the accumulation of materials in the pores and at the surface of the membranes. Thus, when the substance being filtered is contributing resistance to the flow, the extent of membrane fouling can be calculated by resistance in series model[19]

$$\frac{d(v)}{dt} = J_w = \frac{\Delta p}{\mu(R_m + R_p + R_c)} \quad (6)$$

where R_m (m^{-1}) is the membrane hydraulic resistance, R_p (m^{-1}) is the resistance due to pore blocking, and R_c (m^{-1}) is the resistance arising from cake formation.

The membrane resistance, pore-blocking resistance, and cake-layer resistance can be calculated by using the following equations:[30,31]

$$R_m = \frac{\Delta p}{\mu J_{w1}} \quad (7)$$

$$R_p + R_c = \frac{\Delta p}{\mu J_p} - R_m \quad (8)$$

$$R_p = \frac{\Delta p}{\mu J_{w2}} - R_m \quad (9)$$

$$R_c = \frac{\Delta p}{\mu J_p} - \frac{\Delta p}{\mu J_{w2}} \quad (10)$$

J_{w1} is the pure water flux before protein solution filtration, J_{w2} is the pure water flux after cleaning, and Jp is the flux with the filtration of protein solutions.

The protein adsorbed in the pores and primary layer formed on the membrane surface are irreversibly bound and can be removed only by chemical cleaning. The degree of irreversible flux loss caused by irreversible fouling (R_{ir}) is calculated using the following equation:

$$R_{ir} = \left[\frac{J_{w1} - J_{w2}}{J_{w1}}\right] \times 100 \quad (11)$$

But protein multilayers formed are not as strongly bound as the protein adsorbed directly to the membrane.[11] These reversibly deposited protein layers can be swept away by simple washing with deionized water and sonication. The degree of reversible flux loss caused by reversible fouling (R_r) is calculated using the following equation:

$$R_r = \left[\frac{J_{w2} - J_p}{J_{w1}}\right] \times 100 \quad (12)$$

2.4.8. Characterization of the Fouled Membranes by AFM. To study the extent of fouling in different CA/PAI blend membranes, AFM images of the fouled membranes were studied as described in earlier section.

2.4.9. Cleaning of the Fouled Membranes. The membranes after protein filtration were washed with deionized water and subsequently subjected to sonication for 15 min. Sonication was performed by putting the membrane in a sonication bath

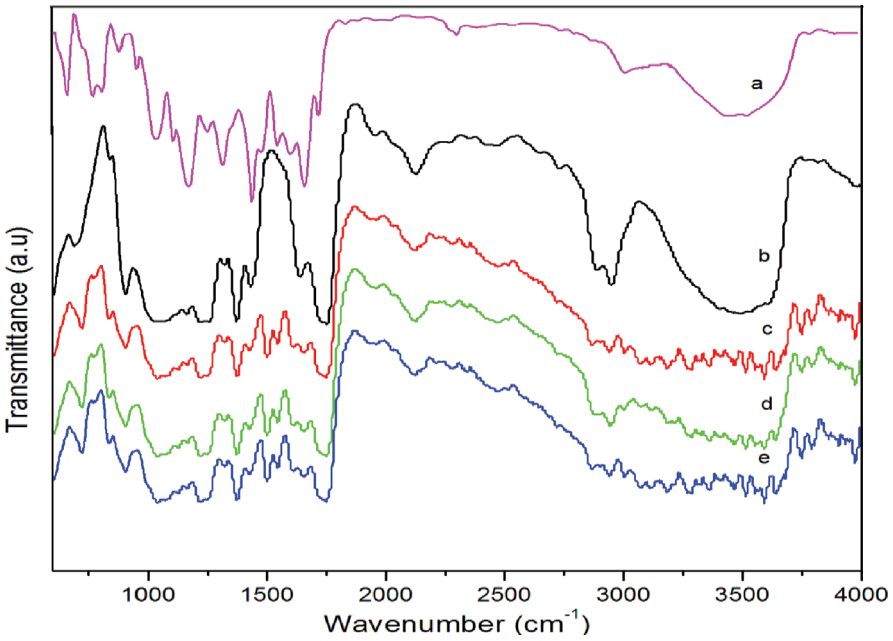

Figure 1. FT-IR spectra of CA/PAI blend membranes and pure PAI powder: (a) pure PAI, (b) 100/0; (c) 90/10; (d) 80/20; (e) 70/30.

(Cole-Palmer 8891) at a frequency of 30 kHz and a bath temperature of 20 °C. The pure water flux of the clean membrane was measured (now denoted as J_{w2}). To evaluate the antifouling property of CA/PAI blend membranes, the flux recovery ratio (FRR) is calculated using the following expression:

$$\text{FRR}\ (\%) = \left[\frac{J_{w2}}{J_{w1}}\right] \times 100 \qquad (13)$$

3. RESULTS AND DISCUSSION

3.1. Fourier Transform Infrared Spectroscopy (FT-IR) Analysis. FTIR spectra of the pure CA, CA/PAI blend membranes, and PAI powder were recorded to investigate the intermolecular interactions between CA and PAI in the blend membranes. FTIR spectra obtained for all membranes and PAI powder are presented in Figure 1. The spectrum of pure CA membrane shows a broad band at 3485 cm^{-1} due to the stretching frequency of −OH group and a sharp peak at 1752 cm^{-1} corresponds to the stretching frequency of −C═O group of CA. On the other hand, spectral bands of pure PAI provide a broad band at 3506 cm^{-1} which corresponds to the stretching frequency of −NH group in the amide linkage. Another two strong peaks with maxima at 1717and 1652 cm^{-1} are ascertained to the stretching frequencies of —C═O group of the amide linkage and —C═O group in the five-membered ring of PAI, respectively.

However, in the CA/PAI blend membranes interesting interactions are revealed due to the shift in the stretching frequencies of above functional groups to higher wave numbers. The spectra of CA/PAI blend membranes indicated that the broad band at 3485 cm^{-1} of pure CA is shifted to 3509 cm^{-1}. Further, the −NH group stretching frequency at 3506 cm^{-1} and —C═O stretching frequency at 1717 cm^{-1} of pure PAI are shifted to 3590 cm^{-1} and 1750 cm^{-1}, respectively, whereas the stretching frequencies of —C═O at 1652 cm^{-1} of PAI and —C═O stretching frequency of CA at 1752 cm^{-1} were unaltered. This shift in the stretching frequencies of CA/PAI blend membranes confirms the establishment of hydrogen bond between the amide group of PAI and hydroxyl group of CA. It could be observed in the spectra of the CA/PAI blend membranes that, with the increase of PAI content, the band at 3485 cm^{-1} became more pronounced with a shift to higher wave numbers. The occurrence of such interactions is initiated by the transfer of a lone pair of electrons present in the nitrogen of amide group. The possible interaction and the established hydrogen bond between CA and PAI in blend membranes are schematically represented in Figure 2. The presence of such —N═H−C−O·····HO— interactions implied a good miscibility of CA and PAI in the blend membranes. The formation of this intermolecular hydrogen bonding favored better compatibility and homogeneity at molecular scale in blend membranes. This type of intermolecular interaction between hydroxyl group of CA and carbonyl group of polyvinyl pyrrolidone has been reported in the literature.[32]

3.2. Scanning Electron Microscopy Analysis of the CA/PAI Blend Membranes. The surface and cross section of the thin film ultrafiltration membranes have a critical role in helping to identify the significance of membrane in the mechanism of selectivity and permeability. It was known that the top layer of membrane is responsible for the permeation or rejection, whereas the sub layer of the membrane acts as a mechanical support.[33]

To understand the influence of PAI composition on the final membrane structure, cross sections of the CA/PAI membranes in the absence and presence of additive were taken using scanning electron microscopy and are shown in Figures 3 and 4, respectively. General structures were very similar for all the membranes consisting of a top skin layer, an intermediate layer with a sponge like substructure, and a bottom layer of fully developed open pores. However, the membranes prepared from CA without PAI exhibit a finger like structure and the pores were not fully opened in the downstream side of the membranes. During the formation process, the structure of the membrane is determined by the instant of phase separation and the volumetric flow rate of solvent and nonsolvent exchange compared to the

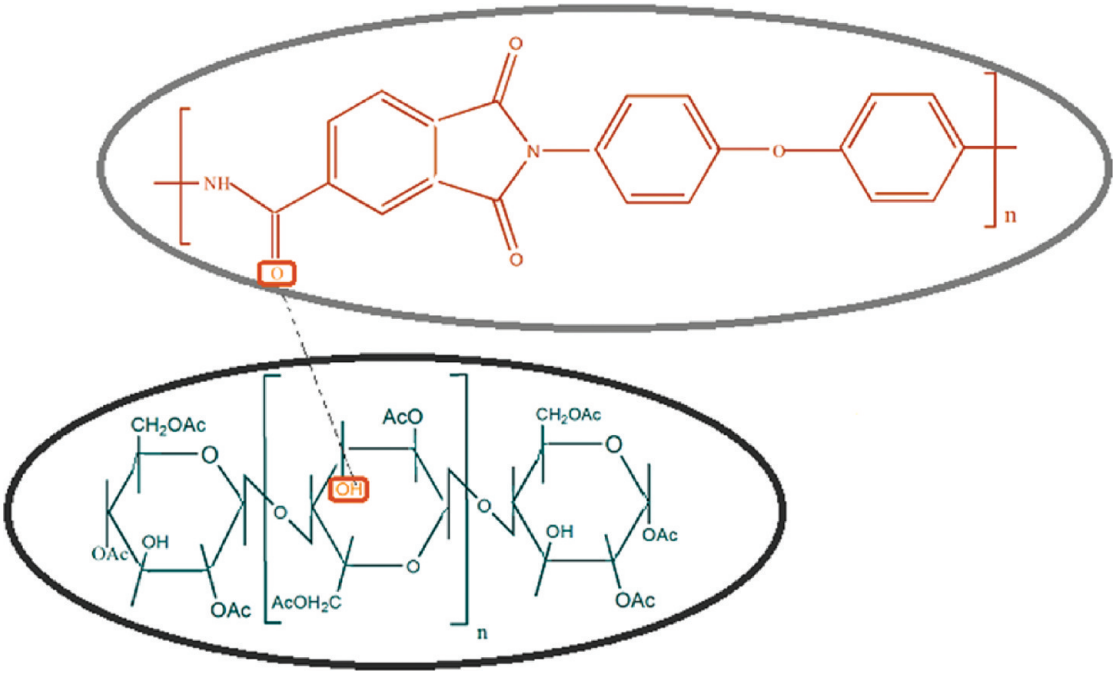

Figure 2. Possible H-bonding interactions between the functional groups of the cellulose acetate and poly(amide-imide) in CA/PAI blend membranes.

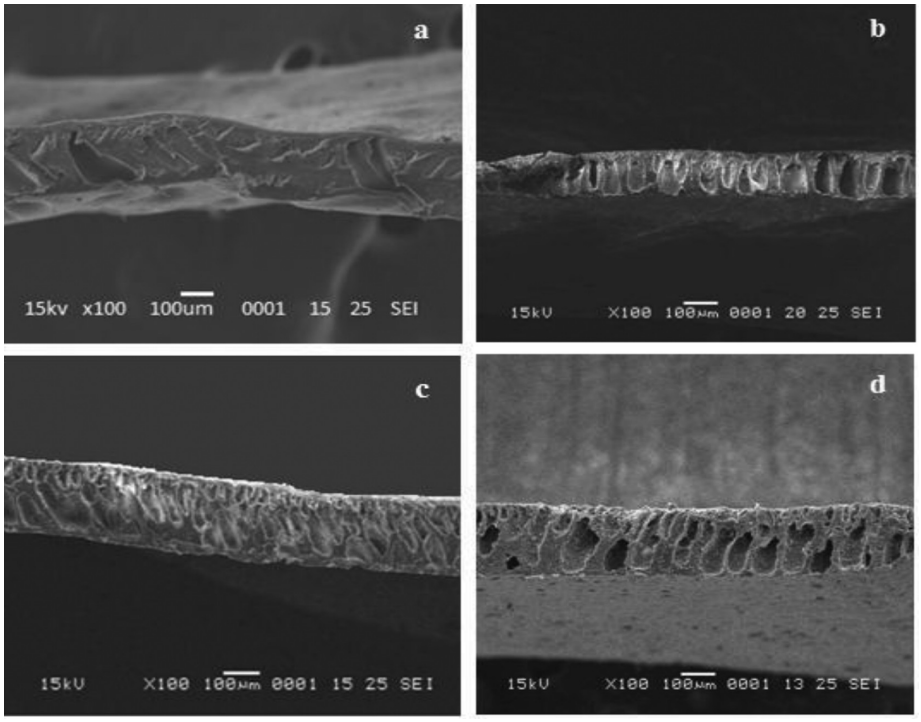

Figure 3. Cross-sectional SEM images of CA/PAI blend membranes (w/w) without additive: (a) 100/0, (b) 90/10, (c) 80/20, (d)70/30.

vitrification rate. In our preparation of membranes, after evaporation of 30 s the cast films were immersed in a coagulation bath of nonsolvent. Upon immersion, nonsolvent (water) moved inward in to the cast film from the nonsolvent bath and this imposed a dramatic increase in the driving force across the polymer-lean nucleus wall. At this time, the polymer-lean nucleus wall allowed water to equilibrate between the internal and external phases before significant outward diffusion of larger solvent molecules. Thus the influx of water was predominantly high compared to the efflux of NMP due to the larger diffusion coefficient of tiny water molecules compared to that of the much bulkier organic solvent molecule.[34,35] But in the case of pure CA membranes, this mutual movement is slow compared to the CA/PAI blend membranes due to the "tortuous" path of the crystalline regions of the CA and this region was considerably decreased in blend films due to the presence of PAI. Thus the osmotic pressure developed inside the polymer-lean

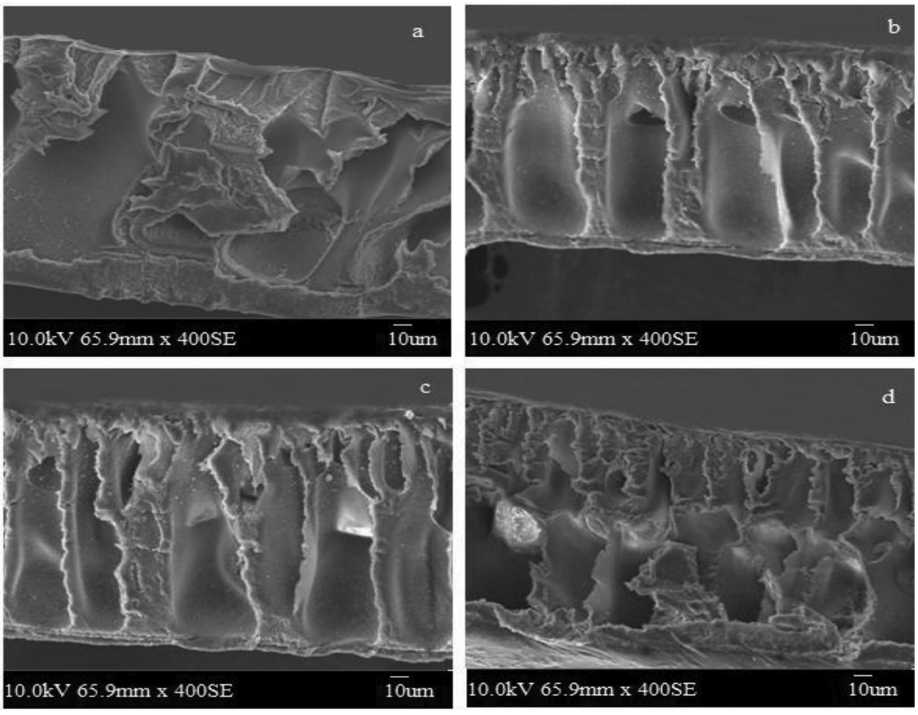

Figure 4. Cross sectional SEM images of CA/PAI blend membranes with 2.5 wt % additive (w/w): (a) 100/0; (b) 90/10; (c) 80/20; (d) 70/30.

droplets of pure CA membranes were not high enough to rupture the walls of these nuclei.

Experimentally, several minutes of coagulation time was needed for "vitrification" of the film made of pure CA, while blend polymers were set in 4−5 min. The longer exchange time between the solvent and nonsolvent in the coagulation bath results in more developed process of polymer-lean phase growth and coalescence, thus the larger finger like pores in pure CA membranes. But in case of blends of CA/PAI, high diffusion rate and hydrophilicity results in the formation of tear like structures with more sponge like areas in the sub layer. However highly open transition sublayer structure were difficult to obtain with pure CA, because the diffusion process associated with the redissolution step was slowed by the viscosity of the polymer solution and the immobilized water layer formed on the water−polymer interface.[36] In contrast to other blend membranes, CA/PAI at 70/30 composition exhibits a fingerlike cavity in the sublayer and macrovoids in the bottom layer. Because of the larger driving force between solvent and nonsolvent, polymers clustered together to exclude solvent within their domains; small pores rapidly grow to form macrovoids. In addition to this, immiscible phase behavior of the blend components largely contributes to this macrovoidal structure, since the segmental gap between the components is high at the 70/30 blend composition.

3.3. Atomic Force Microscopy Analysis of the CA/PAI Blend Membranes. Atomic force microscopy is considered to be more reliable in the characterization of surface features of the membranes, in particular surface roughness of the membranes, which plays a major role in particle fouling during operation. These surface roughness values give insight into the differences in the chemical structure, variations in the local hardness of the hydrophilic/hydrophobic domains, and chemical nature of the membranes surface.

Figures 5 and 6 are atomic force microscopic images of the membranes prepared in the absence and presence of PEG-600, respectively. In these images, the brightest area represents the highest points or nodules of the membrane surface and dark regions indicate the valleys or membrane pores. It seems that, in case of pure CA membranes, the surface contains "nodules" and as the concentration of PAI increases the 'nodules" almost disappeared at 80/20 blend composition. This is due to the high viscosity of the CA casting solution and its highly crystalline structure, which restricts the "valley" formation in pure CA membranes. In the case of CA/PAI blend at 70/30 composition, the "nodules" reappeared once again and it is larger in size. This is because, as the PAI concentration increases, the immiscible nature of the blend increases due to the low adhesion properties between CA and PAI chains. Further, from the AFM images of membranes, it can be observed that when the concentration of dispersed phase increases the morphology becomes more coarse and unstable due to the unfavorable interactions of the components at the interface.[37]

Surface roughness of the membranes which was reported in the preliminary part of the present investigation is tabulated in Table 2, because of its significance in the fouling propensity of the CA/PAI membranes. From the results it was clear that the surface roughness of the membranes decreased with an increase in concentration of PAI in the casting solution. Elimelech and co-workers[38] correlated the surface roughness of the membranes with colloidal fouling and their experiments showed an increase in colloidal fouling at increased surface roughness. A mechanistic explanation for the profound effect of surface roughness on the fouling is intricately related to the nature of the membrane morphology, sublayer resistance, size, shape, and charge of the protein molecules under study. Permeation rate through ultrafiltration membrane is inversely proportional to the thickness of the active layer and thus permeation through a rough membrane will occur at the bottom of the "valley" with thickness increasing toward the peaks. Hence, convection and particle transport in rough membranes are focused towards the bottom of the "valley"

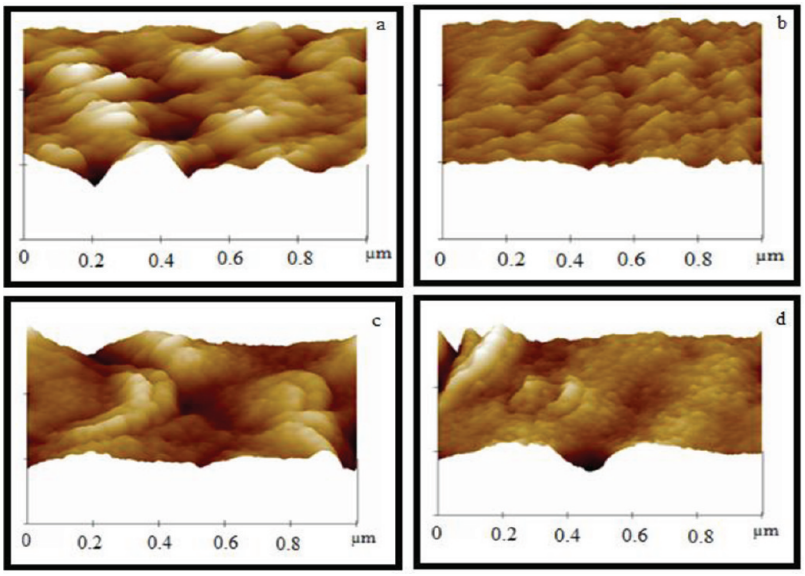

Figure 5. AFM three-dimensional images of CA/PAI membranes (w/w) without additive: (a) 100/0; (b) 90/10; (c) 80/20; (d) 70/30.

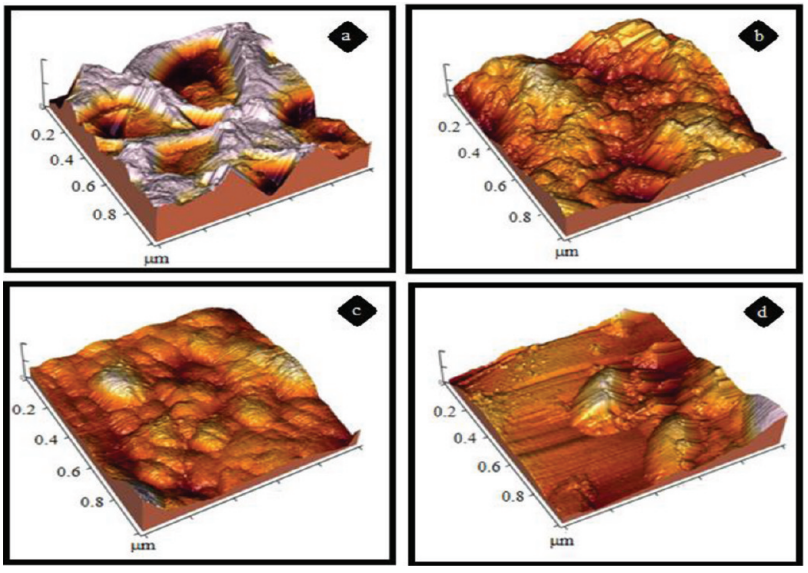

Figure 6. AFM three-dimensional images of CA/PAI blend membranes (w/w) with 2.5 wt % additive: (a) 100/0; (b) 90/10; (c) 80/20; (d) 70/30.

which presents "path of least resistance to permeation".[39] Because these "valleys" are of irregular shape, a lodged particle may not completely plug the pore, but it may significantly restrict the flow through the pore opening. The valleys quickly become clogged with multiple layers of densely packed particles increasing the cumulative resistance to flow in the valleys and leading to more rapid loss of flux than for a smooth membrane. In the case of smooth membranes, even if the same number of particles were deposited, they would likely to be more evenly spaced resulting in less overall flux decline. Thus, for the smooth membrane, until a thick cake layer develops no flux decline will be detected.[38,39] Thus, change in the surface roughness by the incorporation of PAI corresponds to improvement in separation efficiency and fouling resistance of the CA/PAI blend membranes that will be discussed in the subsequent sections.

3.4. Molecular Weight Cutoff (MWCO) and Mean Pore Size. The separation characteristics and pore size of ultrafiltration membranes are usually expressed in terms of the molecular weight cutoff. The MWCO can generally be estimated with linear polymers such as poly(ethylene-glycol) or poly(vinyl-pyrrolidone) or with protein molecules of spherical shape. In the present investigation, spherical proteins of different molecular weight were used for the MWCO determination and the results obtained were compared with that of the linear PEG molecules reported in the first part of the present investigation.[40] The MWCO and mean pore size of the prepared CA/PAI blend membranes in the absence and presence of the additive PEG-600 are tabulated in Table 2. Pure CA membrane has molecular weight cutoff of 45 kDa and it decreased to 20 kDa at 80/20 blend composition without additive. From the observed results, it was

Table 2. Effect of Blend Ratio on the Molecular Weight Cutoff, Average Pore Size, and AFM Surface Roughness of CA/PAI Blend Membranes

polymer blend composition (wt %)	PEG 600 (wt %)	molecular weight cutoff (kDa)	average pore size (nm)		AFM surface roughness data		
			protein	PEG[a]	R_a (nm)	R_q (nm)	R_z (nm)
100/0	0	45	13.20	4.11	6.38	5.03	31.38
90/10	0	35	10.27	3.18	5.11	3.62	23.47
80/20	0	20	5.87	2.84	3.26	2.32	15.57
70/30	0	35	10.27	2.84	2.27	1.59	9.92
100/0	2.5	69	20.24	4.87	7.97	6.43	43.38
90/10	2.5	45	13.20	3.67	6.43	5.31	36.47
80/20	2.5	20	5.87	2.84	4.72	3.84	27.09
70/30	2.5	45	13.20	2.59	5.38	4.02	18.11

[a] Mean pore size calculated from the rejection of PEG molecules.[40]

clear that an increase in PAI composition in the blend membranes decreased the molecular weight cutoff of the membranes.

The decrease in magnitude of the pore size of the CA/PAI blend membranes by the addition of PAI is in clear accordance with the sponge like substructure and lower surface roughness values obtained in SEM and AFM analysis, respectively. As the PAI concentration increases, the less viscous component PAI forms smaller dispersed phase in more viscous CA matrix due to the comparatively restricted diffusion and increased shear stress resulting from the more viscous CA matrix. Thus the availability of more PAI for the formation of small networks with CA leads to the development of super molecular aggregates in the casting solution, which results in the formation of a larger number of small pores. The MWCO and pore size of the CA/PAI membranes increased by the addition of water-soluble additive PEG-600 into the casting solution. The presence of this nonsolvent increases the thermodynamic instability of the casting solution, which leads to the instantaneous demixing of NMP and water during membrane formation resulting in larger pores.[34]

It can be observed from Table 2 that MWCO and pore size obtained with spherical protein molecules are higher than those of the linear PEG molecules. In general, retention depends on a number of factors in addition to the molecular weight of macromolecules such as the size, shape, and conformation, and most importantly the interaction of macromolecule with the membranes. Because particle−membrane and particle−particle interactions are controlled by the physicochemical and hydrodynamic conditions of the filtration process, it is expected that changes in solution chemistry (ionic strength and pH) and particle shape would result in marked changes in rejection behavior. At acidic and basic pH, pores adopt an extended chain conformation due to the electrostatic repulsion between the polymer chains. At our operational pH-6.0, amino groups of PAI in CA/PAI blend membranes get protonated ($\equiv NH_2^+$) and this expected to impart a constant positive charge in the membrane surface and in the pore walls. Because the proteins were negatively charged at this pH (above the isoelectric point pI 4.7, BSA), the electrostatic interaction with the positively charged membranes dragged it close to the membrane surface; under such conditions it is acceptable to observe a rejection lower than what may be expected in the size exclusion. If the solute and membrane surface have an opposite charge, one might expect pore size determined from retention measurements to yield pore size larger than the true size because the pressure driven flow will be facilitated by an

Scheme 1. Schematic Representation of the Interactions Involved in the Rejection of (a) PEG Molecules, Length, *l*, and Radius, r_p, and (b) Protein Molecules, Radius, r_p, in CA/PAI Membranes

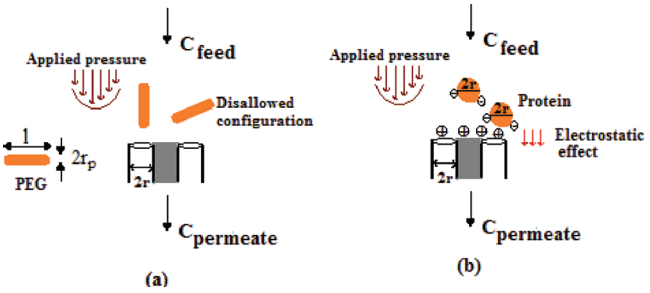

electro osmotic driven flow and vice versa.[41,42] This type of electrostatic driving force was completely absent in the linear PEG molecules due to its inert nature and observed rejection was based on size exclusion only.

Anderson theoretically studied the transport of nonspherical solutes across porous membrane with cylindrical pores, and rejection for rod-shaped particle was predicted to be larger than that for a spherical particle with equivalent molecular weight.[43] In an unbounded fluid, the resistance experienced by a rod with flow parallel to its long axis is expected to be 20−200% larger than that of a sphere with the same diameter. Therefore, the rejections are based solely on configurational effects, i.e., on consideration of the sterically allowed positions and particle orientations in the pore.[41−43] Schematic representation of the various interactions involved in the rejection of linear PEG and spherical protein molecules in CA/PAI membranes are given in Scheme 1. When compared in this manner, the percentage rejection for the rod shaped molecule should be larger than that observed for a sphere with the same diameter. There are two possible explanations for the discrepancy between the observed percentage rejection for spherical proteins and the linear PEG molecules. (i) The fraction of linear PEG molecules approaching the membranes in a direction perpendicular to the orientation of the pore axis is higher and thus particle reflection coefficient would be larger than that observed for a sphere with the same diameter. (ii) Agreement between the percentage rejection for proteins and PEG molecules aligned with the flow is expected only if

Table 3. Percentage Rejection and Permeation Flux Values of the Different Proteins by CA/PAI Blend Membranes

polymer blend composition (wt %)	PEG 600 (wt %)	protein rejection (%)				protein permeation flux (lm^{-2} h^{-1})			
		BSA	EA	pepsin	trypsin	BSA	EA	pepsin	trypsin
100/0	0	88.72	84.91	78.12	76.83	29.80	38.73	44.52	47.69
90/10	0	94.30	90.68	83.45	79.27	45.35	63.25	69.80	78.14
80/20	0	97.95	91.57	85.17	81.15	42.70	61.95	66.10	75.29
70/30	0	93.17	87.81	82.60	78.91	66.20	90.80	101.5	114.8
100/0	2.5	88.62	79.12	77.25	74.39	46.30	56.90	69.72	87.65
90/10	2.5	94.37	85.78	79.32	77.91	68.25	88.50	99.81	106.7
80/20	2.5	96.42	88.71	84.90	80.67	61.52	83.91	92.25	101.3
70/30	2.5	92.56	84.40	79.20	76.50	89.10	103.4	106.2	119.7

hydrodynamic interactions (solution pH) are neglected. However our results indicate that particle orientation in the pore may be the more significant issue, with the alignment of PEG molecules in a direction perpendicular to the orientation of the pore axis leading to its high rejection compared to spherical protein molecules.

3.5. Protein Rejection Studies of the CA/PAI Blend Membranes. Ultrafiltration is considered as a powerful technique for the concentration of protein solutions since it is gentler towards the delicate proteins than conventional separation processes. In the ultrafiltration of proteins, pH is an important parameter since proteins are strongly hydrophobic at their iso-electric point and adsorption on membranes may therefore be increased due to hydrophobic interaction.[43] A protein of low molecular weight, trypsin, was used initially for the ultrafiltration experiments, because it was expected that ultrafiltration of high-molecular-weight protein at the beginning would cause fouling of membrane, which would spoil the originality of the pores for the separation and comparison of low-molecular-weight proteins.[45]

Table 3 shows the rejection behavior of the membranes for all of the above proteins. From the rejection values, it was revealed that as the concentration of PAI in the blend system increases, the rejection of a particular protein increases due to the smaller size of the membrane pores as shown in morphological analysis. The pure CA membranes in the absence of additive exhibited 88.72% rejection for BSA, which was lower than that of the CA/PAI blend membranes. The other proteins EA, pepsin, and trypsin had rejections of 84.91, 78.12, and 76.83% respectively; this higher percentage rejection of BSA and lower percentage rejection of trypsin is obviously due to their molecular sizes. Observed rejection values are substantiated by the finger like pores in the pure CA and sponge like structures in the blend CA/PAI membranes as indicated in Figures 3 and 4. This increase in rejection of the respective proteins was increased up to 80/20 blend composition and further increase in PAI content decreases the rejection. Despite the decrease in rejection values at 70/30 blend composition, these values are higher than those of pure CA membranes. This lower rejection is due to the heterogeneity arising as a result of the higher PAI content creating gaps between the polymer chains. Thus the rejection of a given protein by the membranes was in the order CA/PAI (80/20 wt %)> CA/PAI (90/10 wt %) > CA/PAI (70/30 wt %) > CA (100 wt %). From the rejection values of the membranes with additive, it is revealed that addition of PEG-600 decreased the rejection of all of the protein molecules under study. Introduction of PEG-600 into the casting solution decreases the rejection of the respective proteins and it may be attributed to the rapid leaching out of PEG-600 during gelation to lower the free energy of the system.

3.6. Protein Solution Permeate Flux Studies of the CA/PAI Blend Membranes. The permeate flux of protein solution is essential in predicting the efficiency and economics of the membranes separation process. The permeate flux of proteins such as BSA, EA, pepsin, and trypsin by the pure CA and CA/PAI blend membranes in the absence and presence of additive is shown in the Table 3. The pure CA membranes in the absence of additive showed a protein solution permeate flux value of 29.8 L/m^2h. The other proteins also had lower flux values because of lower porosity (but pore size was high which leads to the lower rejection) and the closed pores in the downstream side of the CA membranes. Even though the pores of the pure CA membranes are larger than those of the CA/PAI blend membranes, they are not equally distributed and did not open up properly in the downstream side of the membranes. Thus the permeate flux values of egg albumin, pepsin, and trypsin were found to be 38.73, 44.52, and 47.69 L/m^2h, respectively. The permeation rates of the different protein solutions presented in Table 3 indicated that the flux values are higher for CA/PAI blend membranes. This was explained by the fact that in the initial stages of filtration, smaller proteins accumulated in these closed pores of pure CA membranes resulting in pore plugging which in turn decreases the flux. This low flux is justifiable, considering the high surface roughness values of pure CA membranes due to the presence of few large pores in the surface of the membrane compared to the CA/PAI blend membranes. For a given blend composition, the addition of 2.5% PEG-600 increased the protein solution permeate flux considerably due to the large pore size of the membranes. The order of flux of the proteins was trypsin > pepsin > EA> BSA and membranes flux was in the order CA/PAI (70/30 wt %) > CA/PAI (90/10 wt %) > CA/PAI (80/20 wt %) > CA (100 wt %).

3.7. Fouling Analysis by BSA. To understand the fouling resistant ability of the prepared membranes, fouling analysis was carried out by BSA as the model protein. Flux decline rate, R_{fd}, was used to evaluate the fouling resistant ability of the pure CA and CA/PAI blend membranes. The lower the value of R_{fd} means higher fouling-resistant ability of the membranes and vice versa. Table 4 shows the initial pure water flux, steady state protein flux, flux decline rate, and pure water flux of the fouled membranes after cleaning. As shown in Table 4, the membranes with 0%, 10%, 20%, and 30% PAI content have R_{fd} value of 89.74%, 89.19%, 90.20%, and 84.41%, respectively. From these flux decline rate values, it was clear that fouling-resistant ability of the CA membranes increased by the addition of PAI into the casting solution.

Under constant pressure separation, considerable decline in permeate flux with time was observed due to concentration polarization

Table 4. Summary of the Pure Water Flux, Initial Protein Flux, Steady State Protein Flux, Water Flux after Cleaning, Flux Decline Rate, and Flux Recovery Ratio of CA/PAI Blend Membranes

		$lm^{-2} h^{-1}$					
polymer blend composition (wt %)	PEG 600 (wt %)	pure water flux, J_{w1}	initial protein flux, J_{p1}	steady state protein flux, J_p	pure water flux after cleaning, J_{w2}	flux decline rate, R_{fd} (%)	flux recovery rate, FRR (%)
100/0	0	80.7	29.80	8.27	60.55	89.74	75.13
90/10	0	106.5	45.35	11.51	87.37	89.19	82.47
80/20	0	140.8	42.73	13.79	130.91	90.20	93.28
70/30	0	167.3	66.20	26.07	148.84	84.41	89.62
100/0	2.5	119.4	46.32	10.85	96.74	90.90	81.67
90/10	2.5	179.1	68.25	14.77	154.00	91.74	86.92
80/20	2.5	256.4	61.50	17.79	235.80	93.06	92.20
70/30	2.5	313.6	89.10	30.98	275.91	90.11	88.17

and adsorption on the membrane surface. In the stirred cell, the mixing induced by the stirring actually swept protein molecules away from the membrane surface and minimized concentration polarization. Hence the binding of proteins on the surface by physical forces such as hydrophobic interaction is predominant in determining its fouling resistance ability. This hydrophobic interaction between the proteins and membranes is at a minimum in blend membranes compared to pure CA membranes, because of the presence of reactive functional groups which minimizes the interfacial energy.[46] Thus the fouling resistance of the blend membranes is improved considerably by the incorporation of PAI due to the preferential orientation of the polar groups towards water during membrane formation process which leads to the enrichment of surface with functional groups. In the case of CA/PAI blend membranes, an ordered structure of water molecules on the membrane surface was formed by the hydrogen bond between the hydrophilic reactive sites and water. For protein to be adsorbed on such a membrane with immobilized bound layer of water, it must first displace the ordered water molecules associated with the surface groups.[47] In CA/PAI blend membranes this water layer keeps the proteins in the bulk solution and minimum availability of such reactive sites for water in pure CA membranes leads to the instantaneous binding of proteins. Schematic representation of the formation of hydration layer in the CA/PAI membranes and its role during protein separation are illustrated in Scheme 2.

Scheme 2. Schematic Representation of the Formation of Hydration Layer in CA/PAI Blend Membranes and Its Role in Protein Separation

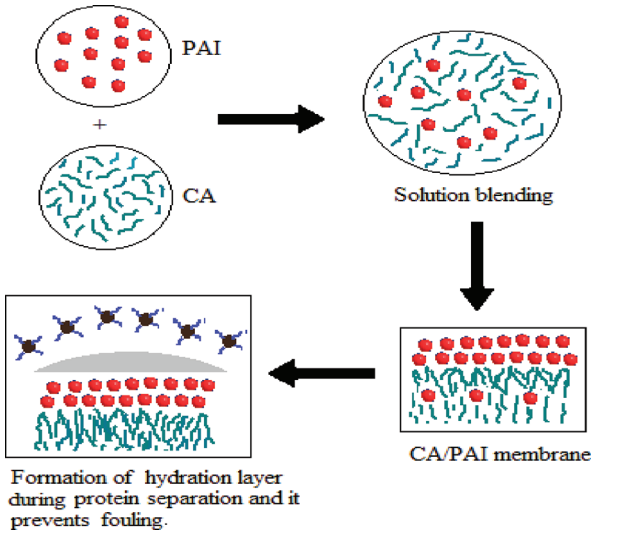

3.8. Fouling Evaluation by Resistance in Series Model. It was established that protein molecules targeted for separation by ultrafiltration tend to be adsorbed onto the surface and into the pores of the membranes. The extent of adsorption depends on the different types of protein−membrane interactions such as hydrophobic interactions, hydrogen bonding, van der Waals interactions, and electrostatic effect.[48,49] Moreover, due to the rejection of proteins by the membrane, there exists concentration polarization near the surface.

Various filtration resistances such as intrinsic membrane resistance (R_m), fouling resistance caused by pore plugging (R_p) and cake layer resistance formed on the surface of the membrane (R_c) of the pure CA and CA/PAI blend membranes during BSA separation are tabulated in Table 5. From Table 5, it can be seen that the hydraulic resistance of the CA membranes is decreased by the incorporation of PAI in to the casting solution. The decrease in hydraulic resistance indicates the difference of both microstructure and morphology of CA/PAI blend membranes; moreover, these membranes have a different cross-section microstructure, pore size, and surface roughness as discussed in previous sections. Similar to hydraulic resistance, the resistance from pore plugging also decreased considerably by the incorporation of PAI and this change can be correlated to the change in pore size of the CA/PAI blend membranes. In CA/PAI membrane at 70/30 composition under the effect of applied pressure, the proteins are easily passed through the pores due to its large size and for pure CA membranes with comparable pore size that of BSA leads to severe pore blockage. Membranes at 90/10 and 80/20 compositions with smaller pore size protect it from pore blockage during BSA separation due to its complete rejection. Cake layer formation on the surface of the membrane follows the same trend as that of pore plugging with a minimum in the blend membranes. Le and Howell observed that physical protein adsorption occurred first on the surface probably as a monolayer, and then further protein build-up took place via intermolecular disulfide bonding and hydrophobic interactions.[50,51] Fast adsorption in pure CA membranes gives less time for protein molecules to spread out at the surface; consequently, area occupied per molecule is lower

Table 5. Summary of the Total Fouling Resistance, Reversible Fouling, and Irreversible Fouling of CA/PAI Blend Membranes during Protein Separation

		in m^{-1}					
polymer blend composition (wt %)	PEG 600 (wt %)	membrane resistance, $R_m \times 10^{10}$	pore plugging resistance, $R_p \times 10^{10}$	cake layer resistance, $R_c \times 10^{10}$	total resistance, $R_t \times 10^{10}$	reversible fouling, R_r (%)	irreversible fouling, R_{ir} (%)
100/0	0	1.73	0.58	14.6	16.91	64.74	25.14
90/10	0	1.31	0.29	10.5	12.10	71.19	18.81
80/20	0	0.99	0.07	9.05	10.11	83.20	07.36
70/30	0	0.83	0.11	4.42	5.36	73.41	11.00
100/0	2.5	1.17	0.27	11.4	12.84	71.90	19.15
90/10	2.5	0.77	0.13	8.53	9.43	77.74	14.29
80/20	2.5	0.54	0.05	7.25	7.84	85.06	08.76
70/30	2.5	0.44	0.06	3.91	4.41	78.11	12.23

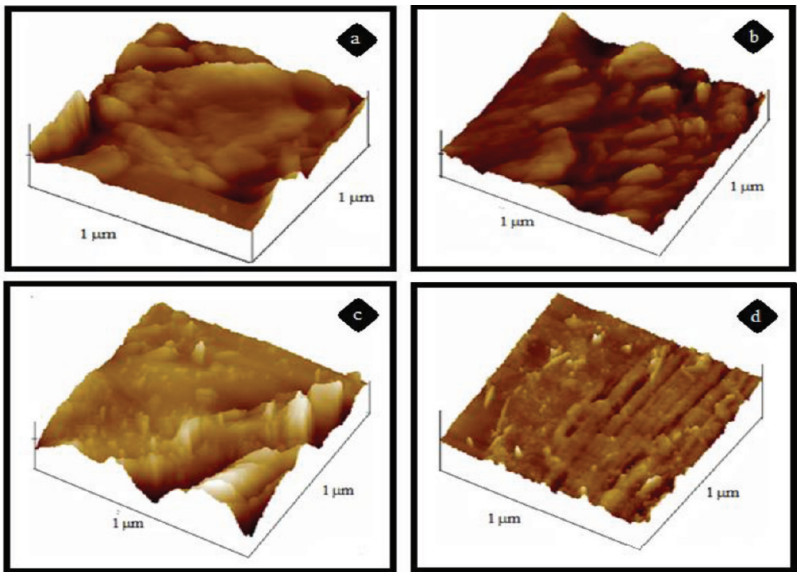

Figure 7. Three-dimensional AFM images of fouled membranes (w/w) without additive after 4 h of protein filtration: (a) 100/0; (b) 90/10; (c) 80/20; (d) 70/30.

and the adsorbed amount is higher. Further, this compact cake formation in pure CA membranes is also related to its high surface roughness. However, the uniform distribution in the blend membranes minimizes the bilateral disulfide bond formation among the protein molecules which leads to the more aligned cake layer protein on the surface.[52]

To study the antifouling property in more detail, we calculated reversible flux decline and irreversible flux decline of the pure CA and CA/PAI blend membranes, and the results are tabulated in Table 5. It can be seen that the R_{ir} value of the pure CA membrane is larger than that of CA/PAI blend membrane and main flux decline is because of irreversible fouling. From this it is clear that CA/PAI blend membrane has a stronger ability to resist membrane fouling than pure CA membranes due to the presence of amide and imide linkages. The existence of PAI on the CA membrane surface increases the hydrophilicity and further reduces protein adsorption and deposition, especially irreversible protein adsorption and deposition. However, the membrane fouling of the CA/PAI blend membrane was largely attributed to reversible membrane fouling, which can be easily removed by simple water washing.[53]

3.9. Atomic Force Microscopic Analysis of Fouled Membranes. The protein coverage in the membrane surface after BSA ultrafiltration has been studied through atomic force microscopy imaging. After R_{ir} and R_r calculation, membranes were again subjected to BSA filtration for 4 h and images of the fouled membranes were taken. Figure 7 represents the three-dimensional AFM images of the fouled CA and CA/PAI blend membranes without additive. Comparison between the images revealed that the structures of the deposited BSA layers at the pure CA and CA/PAI blend membranes are different in shape and size indicating different extent of fouling.[54] Protein adsorption in a polymeric membrane starts with a monolayer formation by the interaction between the membrane surface and proteins, and subsequent layers are formed by the disulfide linkages between the monolayer proteins in the surface and proteins in the bulk solutions. Thus the structure of the monolayer formed on the surface has a profound effect in the final cake formation and resultant flux decline during operation. According to Bowen et al., the protein uniformly covers the more hydrophilic surfaces and nonuniform protein clusters are formed in hydrophobic surfaces due to preferential adsorption at specific sites.[55]

Generally the monolayer of protein formed in ultrafiltration membranes depends on the surface roughness, surface charge

distribution, and hydrophobic/hydrophilic balance. Among these, it is obvious that membrane roughness is the most influential surface property, and in a rough membrane particles are preferentially transported into the valleys and more extensively at hydrophobic sites. Proteins tend to adsorb comprehensively and irreversibly at hydrophobic surfaces than hydrophilic surfaces because of the greater degree of unfolding in the former. In pure CA membranes BSA deposits were compact, because of its high surface roughness and slightly higher hydrophobic/hydrophilic balance arising from the methylene groups which favor deposition followed by unfolding. In contrast, in CA/PAI blend membranes the shape of the BSA deposits was uniform due to the electrostatic protein−surface interactions where proteins are more folded.[56]

3.10. Flux Recovery Ratio of CA/PAI Blend Membranes. Hydraulic cleaning efficiency and fouling-resistant abilities of the membranes were calculated in terms of the flux recovery ratio (FRR). It is well-known that higher value of FRR indicates a higher efficiency of hydraulic cleaning and better fouling resistance property of the membranes. FRR values of the pure CA and CA/PAI blend membranes with PEG-600 are shown in Table 4. FRR values of the pure CA membranes are comparatively lower than those of CA/PAI blend membranes. Thus it can be concluded that the protein deposited on CA membranes is so strong and that could not be removed by hydraulic cleaning. Closed pores of the CA membranes probably induce more BSA adsorption and deposition into the pores which causes more serious membrane fouling. The FRR value of CA/PAI blend membranes is 93.28% at 80/20 composition which means a higher efficiency of hydraulic cleaning and higher antifouling property. The higher FRR value of blend membranes is due to the presence of PAI in the surface and it is well documented in literature that surface active component in a binary blend system migrates into the surface and changes the surface property.[57] If the water state at the surface is similar to that in an aqueous solution or the free water fraction on the surface is sufficiently high, the protein adsorption can be reduced substantially. Thus the fouling caused by protein molecules deposition into the pores is reduced dramatically in blend membranes due to its small size and vicinal water layer present on the surface. These weaker protein deposits could be easily removed from the blend membranes by hydraulic cleaning, which results in high FRR.

CONCLUSION

The present investigation deals with the performance assessment of PAI incorporated CA ultrafiltration membranes in the permeation and rejection of commercially important proteins such as BSA, egg albumin, pepsin, and trypsin. Effect of blend ratio on the morphology, molecular weight cutoff, pore size, protein separation efficiency, and fouling propensity of the blend membranes was evaluated. Morphological analysis of the blend membranes showed that as the weight percentage of PAI in the CA matrix increases defect-free top thin layer and spongy sub layer were formed. AFM study revealed that the surface roughness of the membranes was improved considerably by the addition of PAI in the casting solution and it has played a prominent role in the protein separation. The MWCOs of the CA/PAI blend membranes were decreased by the incorporation of PAI. This is due to the availability of more PAI for the formation of small networks with CA leading to the development of super molecular aggregates in the casting solution, which results in the formation of larger number of small pores. From the rejection behavior, it was revealed that as the concentration of PAI in the blend system increases, the rejection of a particular protein increases due to the smaller size of the membrane pores.

Fouling-resistant ability of the membranes studied by BSA as the model protein shows that as the concentration of PAI in the CA membranes increases, fouling propensity decreases due to the presence of reactive functional groups which minimizes the interfacial energy. In the case of smooth blend membranes, particles deposited were more evenly spaced compared to rough CA membranes resulting in less overall flux decline. Resistance in series model analysis revealed that membrane hydraulic resistance, resistance from pore plugging, and cake layer resistance of the membranes decreased considerably by the incorporation of PAI and this change could be attributed to the change in pore size, hydrophilicity, and surface roughness of the CA/PAI blend membranes. AFM imaging shows that BSA deposits were compact in pure CA membranes, because of high surface roughness and slightly higher hydrophobic/hydrophilic balance. It is proposed that the smooth PAI layer on the CA/PAI blend membrane surface prevents protein molecules from contacting the membrane surface directly by forming a hydration layer, and the protein molecules deposited on the PAI layer could be removed easily by water washing due to the reversible fouling characteristics.

AUTHOR INFORMATION

Corresponding Author

*Tel.: 044-22359136. Fax: 044-22350299. E-mail: mohantarun@gmail.com.

ACKNOWLEDGMENT

We gratefully acknowledge University Grants Commission (UGC), New Delhi, India, for financial assistance. S.S. is thankful to DST, New Delhi for award of DST-PURSE fellowship. We also thank Solvay Advanced Polymers, Alpharetta, GA for providing poly (amide-imide) (Torlon 4000T-HV).

REFERENCES

(1) Geise, G. M.; Lee, H. S.; Miller, D. J.; Freeman, B. D.; Mcgrath, J. E.; Paul, D. R. Water purification by membranes: The role of polymer science. *J. Polym. Sci., Part B: Polym. Phys.* **2010**, *48*, 1685.

(2) Su, Y.; Mu, C.; Li, C.; Jiang, Z. Antifouling property of a weak polyelectrolyte membrane based on poly(acrylonitrile) during protein ultrafiltration. *Ind. Eng. Chem. Res.* **2009**, *48*, 3136.

(3) Reis, R. V.; Zydney, A. Bioprocess membrane technology. *J. Membr. Sci.* **2007**, *297*, 16.

(4) Doyen, A.; Beaulieu, L.; Saucier, L.; Pouliot, Y.; Bazinet, L. Impact of ultrafiltration membrane material on peptide separation from a snow crab byproduct hydrolysate by electrodialysis with ultrafiltration membranes. *J. Agric. Food Chem.* **2011**, *59*, 1784.

(5) Saxena, A.; Tripathi, B. P.; Shahi, V. K. An improved process for separation of proteins using modified chitosan−silica cross-linked charged ultrafilter membranes under coupled driving forces: Isoelectric separation of proteins. *J. Colloid Interface Sci.* **2008**, *319*, 252.

(6) Sivakumar, M.; Mohan, D.; Rangarajan, R. Studies on cellulose acetate polysulfone ultrafiltration membranes. II. Effect of additive concentration. *J. Membr. Sci.* **2006**, *268*, 208.

(7) Rahimpour, A.; Madaeni, S. S.; Mehdipour-Ataei, S. Synthesis of a novel poly (amide-imide) (PAI) and preparation and characterization

of PAI blended polyethersulfone (PES) membranes. *J. Membr. Sci.* **2008**, *311*, 349.

(8) Arthanareeswaran, G.; Sriyamuna Devi, T. K.; Mohan, D. Development, characterization and separation performance of organic-inorganic membranes Part II. Effect of additives. *Sep. Purif. Technol.* **2009**, *67*, 271.

(9) Saxena, A.; Tripathi, B. P.; Kumar, M.; Shahi, V. K. Membrane based techniques for the separation and purification of proteins: An overview. *Adv. Colloid Interface Sci.* **2009**, *145*, 1.

(10) Chan, R.; Chen, V. Characterization of protein fouling on membranes: opportunities and challenges. *J. Membr. Sci.* **2004**, *242*, 169.

(11) Sun, M.; Su, Y.; Mu, C.; Jiang, Z. Improved antifouling property of PES ultrafiltration membranes using additive of silica-PVP nanocomposite. *Ind. Eng. Chem. Res.* **2010**, *49*, 790.

(12) Jones, K. L.; O'Melia, C. R. Ultrafiltration of protein and humic substances: Effect of solution chemistry on fouling and flux decline. *J. Membr. Sci.* **2001**, *193*, 163.

(13) Shirazi, S.; Linn, C.; Chen, D. Inorganic fouling of pressure-driven processes- A critical review. *Desalination* **2010**, *250*, 236.

(14) Nilsson, J. L. Protein Fouling of UF membranes: Causes and consequences. *J. Membr. Sci.* **1990**, *52*, 121.

(15) Combe, C.; Molis, E.; Lucas, P.; Riley, R.; Clark, M. M. The effect of CA membrane properties on adsorptive fouling by humic acid. *J. Membr. Sci.* **1999**, *154*, 73.

(16) Nghiem, L. D.; Coleman, P. J.; Espendiller, C. Mechanisms underlying the effects of membrane fouling on the nanofiltration of trace organic contaminants. *Desalination* **2010**, *250*, 682.

(17) Mahendran, R.; Malaisamy, R.; Mohan, D. Cellulose acetate and polyethersulfone blend ultrafiltration membrane. Part I: Preparation and characterizations. *Polym. Adv. Technol.* **2004**, *15*, 149.

(18) Sourirajan, M.; Matsuura, T. *Reverse Osmosis/Ultrafiltration Process Principles*; National Research Council Canada Publications: Ottawa, Canada, 1985.

(19) Cheryan, M. *Ultrafiltration Handbook*; Technomic Publications Co.: Lancaster, PA, USA, 1986.

(20) Rahimpour, A.; Madaeni, S. S. Polyethersulfone (PES)/cellulose acetate phthalate (CAP) blend ultrafiltration membranes: Preparation, morphology, performance and antifouling properties. *J. Membr. Sci.* **2007**, *305*, 299.

(21) Arthanareeswaran, G.; Thanikaivelan, P.; Raajenthiren, M. Fabrication and characterization of CA/PSf/SPEEK ternary blend membranes. *Ind. Eng. Chem. Res.* **2008**, *47*, 1488.

(22) Xiang, D. Y.; Peng, N.; Chung, T. Formation of cellulose acetate membranes via phase inversion using ionic liquid, [BMIM]SCN, as the solvent. *Ind. Eng. Chem. Res.* **2010**, *49*, 8769.

(23) Vandezande, P.; Li, X.; Gevers, E. M. L.; Vankelecom, F. J. I. High throughput study of phase inversion parameters for polyimide-based SRNF membranes. *J. Membr. Sci* . **2009**, *330*, 307.

(24) Kim, I. C.; Lee, K. H.; Tak, T. M. Preparation and characterization of integrally skinned uncharged polyetherimide asymmetric nanofiltration membrane. *J. Membr. Sci.* **2001**, *183*, 235.

(25) Nagendran, A.; Vijayalakshmi, A.; Lawrence Arockiasamy, D.; Shobana, K. H.; Mohan, D. Toxic metal ion separation by cellulose acetate/sulfonated poly (ether imide) blend membranes: Effect of polymer composition and additive. *J. Hazard. Mater.* **2008**, *155*, 477.

(26) Malaisamy, R.; Mahendran, R.; Mohan, D.; Rajendran, M.; Mohan, V. Cellulose acetate and sulfonated polysulfone blend ultrafiltration Membrane. I. Preparation and characterization. *J. Appl. Polym. Sci.* **2002**, *86*, 1749.

(27) Vijayalakshmi, A.; Lawrence Arockiasamy, D.; Nagendran, A.; Mohan, D. Separation of proteins and toxic heavy metal ions from aqueous solution by CA/PC blend ultrafiltration membranes. *Sep. Purif. Technol.* **2008**, *62*, 32.

(28) Mockel, D.; Staude, E.; Guiver, M. D. Static protein adsorption, ultrafiltration behavior and cleanability of hydrophilized polysulfone membranes. *J. Membr. Sci.* **1999**, *158*, 63.

(29) Nagendran, A.; Mohan, D. Protein separation by cellulose acetate/sulfonated poly(ether imide) blend ultrafiltration membranes. *J. Appl. Polym. Sci.* **2008**, *110*, 2047.

(30) Arguello, M. A.; Alvarez, S.; Riera, F. A.; Alvarez, R. Enzymatic cleaning of inorganic ultrafiltration membranes fouled by whey proteins. *J. Agric. Food Chem.* **2002**, *50*, 1951.

(31) Lee, J.; Ahn, W. Y.; Lee, C. H. Comparison of the filtration characteristics between attached and suspended growth microorganisms in submerged membrane bioreactor. *Water Res.* **2001**, *35*, 2435.

(32) Wu, H.; Fang, X.; Zhang, X.; Jiang, Z.; Li, B.; Ma, X. Cellulose acetate-poly(N-vinyl-2-pyrrolidone) blend membrane for pervaporation separation of methanol/MTBE mixtures. *Sep. Purif. Technol.* **2008**, *64*, 183.

(33) Guillen, G. R.; Pan, Y.; Li, M.; Hoek, E. M.V. Preparation and characterization of membranes formed by nonsolvent induced phase separation: A review. *Ind. Eng. Chem. Res.* **2011**, *50*, 3798.

(34) Li, Z.; Ren, J.; Fane, A. G.; Li, D. F.; Wong, F. S. Influence of solvent on the structure and performance of cellulose acetate membranes. *J. Membr. Sci.* **2006**, *279*, 601.

(35) McKelvey, S. A.; Koros, W. J. Phase separation, vitrification, and the manifestation of macrovoids in polymeric asymmetric membranes. *J. Membr. Sci.* **1996**, *112*, 29.

(36) Rajesh, S.; Maheswari, P.; Senthilkumar, S.; Jayalakshmi, A.; Mohan, D. Preparation and characterization of poly(amide-imide) incorporated cellulose acetate membranes for polymer enhanced ultrafiltration of metal ions. *Chem. Eng. J.* **2011**, *171*, 33.

(37) Bowen, W. R.; Doneva, T. A. Atomic force microscopy studies of membranes: Effect of surface roughness on double-layer interactions and particle adhesion. *J. Colloid Interface Sci.* **2000**, *229*, 544.

(38) Elimelech, M.; Zhu, X.; Childress, A. E.; Hong, S. Role of membrane surface morphology in colloidal fouling of cellulose acetate and composite aromatic polyamide reverse osmosis membranes. *J. Membr. Sci.* **1997**, *127*, 101.

(39) Vrijenhoek, E. M.; Hong, S.; Elimelech, M. Influence of membrane surface properties on initial rate of colloidal fouling of reverse osmosis and nanofiltration membranes. *J. Membr. Sci.* **2001**, *188*, 115.

(40) Rajesh, S.; Shobana, K. H.; Anitharaj, S.; Mohan, D. R. Preparation, morphology, performance, and hydrophilicity studies of poly(amide-imide) incorporated cellulose acetate ultrafiltration membranes. *Ind. Eng. Chem. Res.* **2011**, *50*, 5550.

(41) Baltus, R. E.; Badireddy, A. R.; Xu, W.; Chellam, S. Analysis of configurational effects on hindered convection of non-spherical bacteria and viruses across microfiltration membranes. *Ind. Eng. Chem. Res.* **2009**, *48*, 2404.

(42) Dechadilok, P.; Deen, W. M. Hindrance factors for diffusion and convection in pores. *Ind. Eng. Chem. Res.* **2006**, *45*, 6953.

(43) Anderson, J. L. Configurational effect on the reflection coefficient for rigid solutes in capillary pores. *J. Theor. Biol.* **1981**, *90*, 405.

(44) Liu, S. X.; Kim, J. T.; Kim, S. Effect of polymer surface modification on polymer-protein interaction via hydrophilic polymer grafting. *J. Food. Sci.* **2008**, *73*, 143.

(45) Malaisamy, R.; Mohan, D. R. Cellulose acetate and sulfonated polysulfone blend ultrafiltration membranes. Part III. Application studies. *Ind. Eng. Chem. Res.* **2001**, *40*, 4815.

(46) Hamza, A.; Pham, V. A.; Matsuura, T.; Santerre, J. P. Development of membrane with low surface energy to reduce the fouling in ultrafiltration membranes. *J. Membr. Sci.* **1997**, *131*, 217.

(47) Koelhler, J. A.; Ulbricht, M.; Belfort, G. Intermolecular forces between proteins and polymer films with relevance to filtration. *Langmuir* **1997**, *13*, 4162.

(48) Bowen, W. R.; Calvo, J. I.; Hernandez, A. Steps of membrane blocking in flux decline during protein microfiltration. *J. Membr. Sci.* **1995**, *101*, 153.

(49) Huisman, I. H.; Pradanos, P.; Hernandez, A. The effect of protein-protein and protein-membrane interactions on membrane fouling in ultrafiltration. *J. Membr. Sci.* **2000**, *179*, 79.

(50) Howell, J. A.; Velicangil, O. Theoretical considerations of membrane fouling and its treatment with immobilized enzymes for protein ultrafiltration. *J. Appl. Polym. Sci.* **1982**, *27*, 21.

(51) Nakamura, K.; Matsumoto, K. Protein adsorption properties on a microfiltration membrane: A comparison between static and dynamic adsorption methods. *J. Membr. Sci.* **2006**, *285*, 126.

(52) Sun, S.; Yue, Y.; Huang, X.; Meng, D. Protein adsorption on blood-contact membranes, Review. *J. Membr. Sci.* **2003**, *222*, 3.

(53) Madaeni, S. S.; Mansourpanah, Y. Chemical cleaning of reverse osmosis membranes fouled by whey. *Desalination* **2004**, *161*, 13.

(54) Ang, W. S.; Elimelech., M. Protein (BSA) fouling of reverse osmosis membranes: Implications for wastewater reclamation. *J. Membr. Sci.* **2007**, *296*, 83.

(55) Bowen, W. R.; Doneva, T. A.; Stoton, J. G. Protein deposition during cross-flow membrane filtration: AFM studies and flux loss. *Colloids Surf., B* **2002**, *27*, 103.

(56) Dickinson, E. Adsorbed protein layers at fluid surfaces: interactions, structure and surface rheology. *Colloids Surf., B* **1999**, *15*, 161.

(57) Taurozzi., J. S.; Crock, C. A.; Tarabara, V. V. C_{60}-Polysulfone nanocomposite membranes: Entropic and enthalpic determinants of C_{60} aggregation and its effect on membrane properties. *Desalination* **2011**, *269*, 11.